MONITORING PHYTOPLANKTON BIOMASS AND SURFACE TEMPERATURES OF SMALL INLAND LAKES BY MULTISPECTRAL AND THERMAL UAS IMAGERY

A THESIS
SUBMITTED TO THE FACULTY OF THE
UNIVERSITY OF MINNESOTA
BY

GARRETT BARTELT

IN PARTIAL FULFILLMENT OF THE REQUIREMENTS
FOR THE DEGREE OF
MASTER OF SCIENCE

MIKI HONDZO

AUGUST 2021

Acknowledgements

This project would not have been completed without all the people and organizations that have helped me along the way.

First, I would like to thank my friends and family for their support. Their encouragement and love gave me the determination to finish. Thank you for reading my paper, listening to me practice, and giving me constructive criticism when I needed it.

Secondly, I would like to thank my sister, my girlfriend, my mother, my therapist, and all healthcare workers that have been keeping us safe and sane throughout the COVID-19 pandemic.

Lastly, I would like to thank the faculty of the CEGE department at the University of Minnesota. I would not be here without the support, academically and financially, of the department over the last 18 months. I would like to thank Judy Yang and her students, for sharing the eco-lab and the spectrophotometer throughout my project. And thank you to my advisor, Miki Hondzo, for this project and guidance in research and in life.

Table of Contents

Acknowledgements i

Table of Contents ii

Abstract iii

List of Figures iv

List of Tables and Graphs v

1. Introduction 1
    1.1 Harmful Algal Blooms 1
    1.2 Remote Sensing 2
    1.3 UAS Technology 4
    1.4 Site Selection 7

2. Materials and Methods 9
    2.1 Mission Planning 9
    2.2 UAS Data Collection 10
    2.3 In-situ Data Collection 14
    2.4 Chlorophyll-a Extraction 15
    2.5 UAS Data Processing 16

3. Results 20
    3.1 In-situ Measurements 20
    3.2 Chlorophyll-a Measurements 21
    3.3 UAS Flight and Data 22
    3.4 Spectral Indexes and Chlorophyll-a 23
    3.5 UAS Thermal Temperatures 28

4. Discussion 33
    4.1 UAS Determination of Algae Concentration 33
    4.2 UAS Determination of Surface Water Temperature 35
    4.3 Conclusions 37

5. Bibliography 40

List of Figures

FIGURE 1: Satellite photo of Brownie Lake and the surrounding lakes. Image captured by Landsat Copernicus and viewed using Google Earth.

FIGURE 2: A drone photo captured of the cyanobacteria HAB in Cedar Lake in the spring of 2020. Cedar Lake is seen on the right and is a brown color, while the surrounding lakes are not (Cardwell, 2020).

FIGURE 3: DJI Inspire 2 without sensor attached.

FIGURE 4: Brownie Lake survey mission in the DJI Pilot application.

FIGURE 5: Attaching MicaSense Altum camera to DJI Inspire 2.

FIGURE 6: Photo showing Altum specifications from MicaSense User Guide (MicaSense, 2021).

FIGURES 7 and 8: Canoe path taken on Brownie Lake and Hydrolab sample locations. Path and Hydrolab sample locations were visualized using Google Earth

FIGURE 9: Image overlap of the orthomosaic of Brownie Lake. Image generated by Pix4D Quality Report.

FIGURE 10: Contour map of chlorophyll concentration in Brownie Lake.

FIGURES 11 and 12: NDVI with buffer zone 20 and 34. Zone 20 and 34 were marked as outliers by the Thompson Tau test. Leaves can be seen as yellow pixels near the zones and along the shoreline.

FIGURE 13: Thermal temperature map of Brownie Lake post regression analysis**.**

List of Tables and Graphs

TABLE 1: Wavelengths and bandwidths for all sensors. Table from Altum integration guide (MicaSense, 2020).

TABLE 2: Multispectral indexes used in chlorophyll-a analysis with reference index literature.

TABLE 3: Statistics of water quality data collected by the Hydrolab.

TABLE 4: R^2 values for linear regression of each band index listed.

GRAPH 1: Linear relationship between chlorophyll extraction and phycocyanin concentration measured by the Hydrolab.

GRAPH 2: Correlation between chlorophyll-a concentration and mean NDVI pixel value.

GRAPH 3: Histogram showing the range of chlorophyll-a concentrations in Brownie Lake per pixel (20.9 cm^2). Pixel frequency is the number of pixels with the corresponding chlorophyll-a value.

GRAPH 4: Raw LWIR pixel data converted to °C from Centikelvin.

GRAPH 5: UAS collected temperatures versus Hydrolab probe measured temperatures.

GRAPH 6: Histogram of water temperatures in Brownie Lake, post regression analysis. Pixel frequency is the number of pixels with the corresponding temperature value.

Abstract

Chlorophyll-a is an essential environmental indicator for water quality monitoring, as it is used in photosynthesis by all phytoplankton. Chlorophyll-a concentration in water is correlated to phytoplankton biomass, which is used to monitor harmful algal blooms (HABs). The eutrophication of waters observed during HABs can deplete the water of dissolved oxygen, smother aquatic vegetation, and some species can even release cyanotoxins into the environment. Nutrient pollution and warmer waters caused by climate change are expected to increase the intensity and frequency of HABs. Remote sensing chlorophyll-a concentration for HAB monitoring has been demonstrated with satellite imagery. Satellites effectively monitor temperatures and large algal blooms in oceans and large lakes but lack the spatial resolution to monitor small bodies of water effectively.

This study aims to apply remote sensing techniques to multispectral and thermal images captured by an unmanned aerial system (UAS). A UAS survey was conducted on a small freshwater lake, Brownie Lake, in Minneapolis, Minnesota. The collected imagery was then correlated to in-situ chlorophyll-a and temperature measurements.

Data was collected using the MicaSense Altum sensor. The Altum is a combination multispectral and thermal camera designed for agricultural data collection. While the multispectral camera attachment is not designed for surface water surveys, this study observed good agreement between measured chlorophyll-a concentrations in a small freshwater lake and the UAS multispectral data. Chlorophyll-a concentration was discovered to be highly correlated with the indexes containing the near-infrared (NIR) band, with a wavelength of 840 nm. Of the multispectral indexes evaluated in this study,

the most correlated index was the normalized difference vegetative index (NDVI), with an R^2 value of 0.80.

Remotely determined water surface temperatures also showed a correlation to manually collected water temperatures. This correlation was not as definitive, with an experimental R^2 value of 0.31. This research supports the use case for UAS technologies in measuring water quality indicators important to HAB monitoring, such as temperature and chlorophyll-a concentration.

1. Introduction

1.1 Harmful Algal Blooms

Every year around the world, harmful algal blooms (HABs) have threatened the health of citizens, ecosystems, and economies. HABs are overgrown colonies of naturally occurring algae or cyanobacteria that harm the environment, animals, and people (Crabb, 2020). The eutrophication of water can occur in both fresh and coastal waters. There are many causes for HABs, some natural and some unnatural. The harm caused by the excess growth of these algae can remove dissolved oxygen, block out sunlight, clog the gills of aquatic animals, and release toxic compounds into the water (National Oceanic and Atmospheric Administration, 2016). The most common types of phytoplankton associated with HABs are dinoflagellates, diatoms, and cyanobacteria. (Kislik et al., 2018). Although cyanobacteria are bacteria and not algae, they are commonly referred to as blue-green algae. Blooms of cyanobacteria are particularly problematic because cyanobacteria produce cyanotoxins (Kwon et al., 2019), which can be deadly to animals and even humans in rare cases.

Large blooms of algae occur when the algae have access to sunlight, nutrients, and calm water. Plant fertilizers and manure used in agriculture contain the same nutrients that algae need to grow, nitrogen and phosphorus. Water runoff containing plant fertilizers can exacerbate the growth of algae colonies, potentially leading to a bloom. Nutrient runoff is of particular concern in the great lakes of the US, where there is an abundance of agriculture and freshwater lakes (Schmale et al., 2019). Algal blooms have threatened those directly exposed and also affected people who rely on surface water to

access clean water. HABs can drastically increase the price of water treatment or make surface water unsuitable for treatment. In 2014, half a million people in the state of Ohio did not have access to clean drinking water when a HAB of cyanobacteria occurred in the western portion of Lake Erie (Obour et al., 2014). The cyanobacteria bloom released dangerous levels of microcystin into Lake Erie, which contaminated the public water supply in the city of Toledo. Microcystin is a cyanotoxin that can cause serve liver damage (Schmale et al., 2019). Due to climate change and industrial farming, HABs are predicted to become more frequent and more intense (US EPA, 2020). Developments in monitoring and predicting HABs have become increasingly important.

1.2 Remote Sensing

One of the methods used in monitoring blooms is remote sensing. Satellites have been used to track algae blooms starting in 1987, when satellite data collected by the polar-orbiting environmental satellites from the National Oceanic and Atmospheric Administration (NOAA) was used to monitor a red tide caused by a bloom of Karenia brevis off the Atlantic coast of the United States (NOAA NESDIS, 2015). Many technologies and analysis methods have been developed to monitor and forecast HABs from satellites. Sensors carried by satellites are typically multispectral, indicating that they capture the reflectance of multiple wavelengths of light. Reflectance images are captured by the satellite at various wavelengths of light, and each wavelength is called a band. Physical and chemical characteristics of bodies of water can be determined by the amount of light reflected and absorbed at specific frequencies. The reflectance images of different wavelengths are then combined in various arrangements to give spectral

indexes. The physical and chemical characteristics of the body of water are determined by these indexes. Chlorophyll-a concentration, turbidity, and depth are some of the most common water quality indicators determined by remote sensing via satellites (Wynne et al., 2018**)**.

Chlorophyll-a is one of the most important indicators when remote sensing HABs. Chlorophyll-a is a photosynthetic pigment used in photosynthesis and is present in all phytoplankton. Since it is present in all photosynthetic aquatic organisms, chlorophyll-a concentration is used to indicate phytoplankton biomass. Chlorophyll-a, and therefore phytoplankton biomass, can be derived from the water surface reflectance values at specific wavelengths. Maximum absorption for chlorophyll-a is measured at 442.5 nm, with high absorption also measured at 665 nm (Wynne et al., 2018**)**. The highest reflection for chlorophyll-a is measured at 560 nm and 700 nm (Wynne et al., 2018**)**.

The multispectral sensors aboard satellites are often not explicitly catered to measuring water quality indicators. Therefore, multiple different indexes have been developed for measuring chlorophyll-a concentrations, depending on the available bands aboard the satellite. Other limitations to using satellites for water quality data have been identified, such as low spatial resolution, atmospheric and weather interference, and being dependent on satellite location. Clouds can often cover entire lakes, making data collection from satellites impossible in certain weather conditions. Many of the satellites used for monitoring water are also optimized for monitoring oceans, where cloud cover is less of an issue (Kislik et al., 2018).

The average ground sample distance (GSD) for satellites ranges from 10-30 meters (Choo et al., 2018). Ground sample distance is defined as the distance between the

center of two neighboring pixels. With a GSD of 10-30 meters, satellite pixels cover an area between 100-900 square meters. Due to the low spatial resolutions of satellites, many lakes or rivers that experience HABs are too small to be properly surveyed by satellite. The low-resolution leaves satellites best suited for monitoring oceans and large lakes.

Atmospheric effects also can interfere and make data harder or impossible to be interpreted correctly. Water surface temperature is one indicator exceptionally intertwined with weather and atmospheric effects. The water temperature of the oceans is commonly monitored by satellite. Remotely sensing ocean temperatures allow for the observation of ocean currents, coastal upwelling, and the rise of temperatures due to climate change (Fricke et al., 2021). Water temperature is a valuable indicator on small water bodies as well. For HAB monitoring, temperature data can be used to determine if the water is warm enough to support an algal bloom. HABs often require on-demand, up-to-date information to be handled appropriately (Kislik et al., 2018). Quickly receiving data can be hard to accomplish from satellites that may not be positioned correctly.

1.3 UAS Technology

Unmanned Aerial Systems (UASs), or drones, are a widely available, recently developed remote sensing technology that is well equipped to produce high resolution, non-cloud dependent, and on-demand water quality data. UAS technology has already been implemented into many aspects of environmental monitoring, such as forestry, topography mapping, and agriculture. Both multirotor and fixed-wing UASs have been used in agricultural monitoring. Multi-rotor UASs are easy to use and allow for precise

movements, hovering, and vertical launching and landing (Tmušić et al., 2020). A fixed-wing UAS can cover a larger area than a multi-rotor UAS due to the wing's utilization of lift forces. Fixed-wing designs are optimal for larger survey areas free from obstacles (Tmušić et al., 2020). The high spatial resolution make UASs well equipped to monitor small bodies of water.

Multispectral and thermal sensors have been developed that easily attach to UASs. The multispectral sensor attachments for UASs are commonly used in agriculture to measure chlorophyll concentrations in leaves. This allows farmers to assess crop vigor or to identify diseased plants. UAS imagery has more uses than only chlorophyll measurements. The UAS multispectral data is turned into multispectral indexes, giving a wide variety of observable data. The multispectral indexes can determine water distribution, fertilizer management, phenotyping, weed detection, and other important agricultural data, all from a single UAS flight (Simpson et al., 2021).

While the UAS multispectral sensors are optimized for agriculture, recent studies indicate that many agricultural indexes can be used to identify chlorophyll-a concentration water. The agricultural indexes used in this study have already been developed to measure chlorophyll concentrations in leaves. Some of the commonly used agricultural indexes evaluated in this study include the Normalized Difference Vegetative Index (NDVI), the Normalized Difference Chlorophyll Index (NDCI), and Normalized Difference Red Edge (NDRE) index.

The sensor used in this study is the MicaSense Altum. The Altum is a high-resolution, multispectral camera that also contains a long wave infrared (LWIR) thermal sensor. This allows the camera to collect multispectral data in conjunction with thermal

data. The thermal sensor is the FLIR Lepton 3.5, a radiometric capable camera often attached to smartphones. The sensor works by detecting and recording thermal radiation. Thermal radiation is electromagnetic radiation emitted by heat. The light from normal environmental temperatures is low energy radiation; thus, it can be detected in the long-wave infrared range. The thermal sensor is calibrated in-house by FLIR, the thermal camera manufacturer (FLIR, 2018). Currently, most UAS sensors available for purchase are either only multispectral or only thermal. The combination of thermal and multispectral sensors provides more data, insight, and decreases sample collection duration.

With the thermal data, the temperature of the water surface can be measured and monitored. The water temperature is very important, as it often determines the rate of chemical and biological processes in lakes (Jensen et al., 2012). Temperature flux and water mixing can be observed with thermal data (Fricke et al., 2021). The flow of water temperature can help identify wherein the body of water algae might aggregate.

This study attempted to assess the use case for using UAS technology in monitoring algae concentrations and water surface temperatures. UASs provide comparatively low-cost, high-resolution remote sensing data that can be collected regardless of cloud cover. The added flexibility provided by UASs allows for the surveying and monitoring of small water bodies. In-situ measurements of chlorophyll-a concentrations and temperatures of a small lake in Minneapolis, Minnesota, were collected and compared against drone collected multispectral indexes and thermal temperatures.

1.4 Site Selection

The lake examined in this study was Brownie Lake, a small freshwater lake in Hennepin County, Minnesota. Brownie Lake is the northmost lake of the Minneapolis chain of lakes and is attached to Cedar Lake by a canal. Cedar Lake is more commonly used for recreation by the residents of Minneapolis than Brownie Lake. In early spring 2020, a rare HAB of cyanobacteria occurred on Cedar Lake (Crabb, 2020). In places with cold winters like Minnesota, spring waters are typically too cold to support cyanobacteria blooms (Woźniak et al., 2016). This bloom of cyanobacteria made the water hazardous to people and their pets. The cyanobacteria left Cedar Lake a brown color, similar to paint. Cyanobacteria were also the preferred phytoplankton when selecting lakes for this study because the in-situ data were collected with an OTT Hydrolab equipped with a blue-green algae sensor. The blue-green algae sensor measures the water concentration of phycocyanin. Phycocyanin is a photosynthetic pigment specific to cyanobacteria. The blue-green sensor is recommended by OTT Hydromet for freshwaters with large cyanobacteria populations (Sanders et al., 2000).

As of August 2021, no algal bloom has been reported on Cedar Lake or Brownie Lake. Brownie Lake's size and proximity to Cedar Lake made it an ideal candidate for this study. Brownie Lake is 9.28 acres, which allowed for the entire lake to be surveyed in a single UAS flight. The lake is mesotrophic, with a reported trophic state index value of 58 by the Minnesota Department of Natural Resources (MN DNR, n.d.). Although not eutrophic, the lake still contained detectable chlorophyll-a and phycocyanin concentrations.

FIGURE 1: Satellite photo of Brownie Lake and the surrounding lakes. Image captured by Landsat Copernicus and viewed using Google Earth.

FIGURE 2: A drone photo captured by John Cardwell of the cyanobacteria HAB in Cedar Lake in the spring of 2020 (Cardwell, 2020). Cedar Lake is seen on the right and is a brown color, while the surrounding lakes are not.

2. Materials and Methods

2.1 Mission Planning

The UAS used for data collection was a DJI Inspire 2, shown in FIGURE 3. The Inspire 2 is a multirotor UAS. The multirotor design was selected for this survey as it does not need much space for takeoff and landing. Multiple rotors allowed for precise movements and short turnaround distance while the flight was conducted (Kislik et al., 2018).

The flight plans were created using the DJI Pilot application prior to data collection. The survey consisted of the entire lake. A linear flight speed of 5 m/s, an above-ground height of 100 m, a GSD of 4.32 cm/pixel, a side lap ratio of 70%, and a front overlap of 80% were the specifications used to plan the UAS survey. Image overlap is the ratio of the area collected in one image to its neighboring image. Obtaining a high front overlap, 80% or above, was critical if photo alignment and photo stitching errors were to be avoided (Simpson et al., 2021). MicaSense recommended an overlap of no less than 75% (MicaSense, 2020). Turn around distance was set to zero meters to shorten the time of flight. The height of 100 meters was chosen to shorten the flight time, increase the overlap between photos, and decrease the flight distance while maintaining high resolution.

FIGURES 3 and 4: DJI Inspire 2 without sensor attached (left). Brownie Lake survey mission in the DJI Pilot application (right).

2.2 UAS Data Collection

Weather conditions were collected before the flight to ensure the conditions were safe for conducting the UAS survey. Photographic data was collected using the MicaSense Altum sensor, which is equipped with six different sensors, each sensitive to one wavelength of the electromagnetic spectrum. There are five multispectral bands recorded by the MicaSense Altum, blue, green, red, red edge, near-infrared, and a thermal sensor measuring LWIR. The Altum reported image resolution for the multispectral bands is 2064 x 1544, while the thermal sensor reported resolution is 160 x 120 (MicaSense, 2021). The width of the bands is listed in Table 1.

Band	Center	Band Width	Range
Blue	475 nm	32 nm	443-507 nm
Green	560 nm	27 nm	533-587 nm
Red	668 nm	16 nm	652-684 nm
Red Edge	717 nm	12 nm	705-729 nm
NIR	842 nm	57 nm	785-899 nm
Thermal	11 µm	6 µm	5-17 µm

TABLE 1: Wavelengths and bandwidths for all sensors. Table from Altum integration guide (MicaSense, 2020).

The camera collected six images every time it was triggered, creating one image for each band. Each image was numbered with its respective band number. The images collected by the camera were the reflectance measured by the sensor for its individual wavelength. Since each sensor only captured a single band of light, the photos collected are monochromatic. The pixel values for the first five bands are normalized, ranging between 0.00-1.00, with 0.00 indicating no light was reflected and 1.00 indicating all light was reflected. The LWIR thermal band was recorded in units of Centikelvin (*MicaSense Knowledge Base*, 2021). The LWIR sensor is reported by MicaSense to have an accuracy of +/- 5 K and a thermal sensitivity <50 mK.

The images collected from the camera were stored on a flash drive that was plugged directly into the camera. All photos had to be geotagged in order to properly processed data. The MicaSense Altum DJI Skyport Kit came with an embedded global positioning system (GPS) that automatically geotags the location of each photo captured

by the camera. The GPS sensor, named the Downwelling Light Sensor (DLS 2.0), was used to measure the sun irradiance (MicaSense, 2020). The DLS is equipped with 12 directional sensors and eight light sensors. The DLS recorded ambient light conditions and the angle of the sun. The DLS data is essential, as it is used to correct for midflight changes in cloud cover. The DLS data is automatically embedded into the metadata of the images captured by the Altum.

FIGURE 5: Attaching MicaSense Altum camera to DJI Inspire 2.

FIGURE 6: Photo showing the MicaSense Altum and DLS 2.0 specifications from MicaSense User Guide (MicaSense, 2021).

The camera communicated with the controller via a Wi-Fi signal produced by the camera. Settings were established using the MicaSense camera web application. The controller needed to be connected to the camera's Wi-Fi signal to access the web application. The application can be found on the web configuration page described in the User Guide for MicaSense Sensors (MicaSense, 2021). The automatic photo capture setting was set to overlap mode, with a specified image overlap of 80%. The web application allowed for images of the calibration panel to be manually captured. Calibration photos were collected before and after data collection. The calibrated photos were crucial, as this allowed each band's reflectance to be calibrated properly. The camera manufacturer, MicaSense, provided the specific reflectance values for the panel for each wavelength.

2.3 In-situ Data collection

An OTT Hydrolab equipped with a blue-green algae sensor was used to collect phycocyanin concentration in Brownie Lake. The blue-green algae sensor measures in vivo phycocyanin by fluorescence. The intensity of phycocyanin fluorescence is detected by the sensor and recorded as a voltage. The voltage measured by the sensor is proportional to the phycocyanin concentration in the water, and phycocyanin is heavily correlated with cyanobacteria biomass (Sanders et al., 2000).

FIGURE 7: Hydrolab sondes (above) and fluorescence sensors (bottom left) (Sanders et al., 2000).

The probe was calibrated with pH buffers 4.0 and 7.0 before data collection. Distilled water was also used to calibrate phycocyanin to 0.0000 volts. Hydrolab was attached to a canoe and dragged through Brownie Lake while GPS recorded the route.

The recorded data from the Hydrolab was exported to a spreadsheet. In the field, the Hydrolab recorded time, pH, temperature °C, dissolved oxygen, and phycocyanin concentration of the lake every 30 seconds. DO and pH levels were important for knowing how to properly store the lake samples.

Lake water samples were collected for chlorophyll-a analysis, and their GPS coordinates were recorded. GPS recorded position once every second. The GPS output a KML file that was then used to visualize the canoe path in GIS software. The times recorded by the Hydrolab and GPS were aligned. Matching the clocks of the GPS and the Hydrolab allowed the GPS location of each Hydrolab sample to be determined.

2.4 Chlorophyll Extraction

The volume of lake water sampled was large enough to create one chlorophyll-a sample from each lake water sample. Samples were analyzed for chlorophyll-a using the chlorophyll-a extraction method found in the 19th edition of Standard Methods for the Examination of Water and Wastewater (*Standard Methods for the Examination of Water and Wastewater*, 1995). Samples were stored in accordance with the procedure. Lake samples were extracted by filtering the lake water through a Whatman GF/F 0.7 µm glass filter. The glass filters were then ground in a tissue grinder to break down the cell membranes. The slurry, resulting from the grinding of the glass filter, was extracted into 90% acetone and 10% concentrated $MgCO_3$ solution. Samples were then clarified by centrifuge and diluted to a fixed volume of 10 mL. The samples were analyzed by spectrophotometer with 3 mL of the extract contained in 1 cm pathlength cuvettes. Absorbance was measured at 750 nm and 664 nm. The 3 mL of extract was then acidified

with 0.1 mL of 0.1 N HCl. After the sample had been acidified for 90 seconds, absorbance was measured again, this time at 750 nm and 665 nm. Chlorophyll-a concentration was calculated using the following equation and the measured absorbance values (*Standard Methods for the Examination of Water and Wastewater*, 1995).

$$Chlorophyll - a\ (mg/m^3) = 26.7 * \frac{(664_b - 665_a) * V_E}{V_s * L}$$

Where: $664_b = \text{ABS}(664) - \text{ABS}(750)$; prior to acidification.
$665_a = \text{ABS}(665) - \text{ABS}(750)$; after acidification.
V_s = Sample volume (m^3)
V_E = Extract volume (L)
L = Cuvette path length (cm)

The acidification procedure was conducted to ensure no interference from pheophytin in the calculation, a degradation product of chlorophyll-a. The hydrochloric acid removes the Magnesium ion from chlorophyll-a and converts it into pheophytin (*Standard Methods for the Examination of Water and Wastewater*, 1995). The measured sample data was then ready to be compared against the in-situ Hydrolab data.

2.5 UAS Data Processing

The UAS collected photos were stitched together using the Pix4Dmapper software (*Pix4Dmapper 4.1 User Manual*, 2021). The options selected on the software were those recommend on the MicaSense knowledge database on the webpage *How to Process MicaSense Sensor Data in Pix4D* (*MicaSense Knowledge Base*, 2021). Multispectral images were calibrated using the panel photos collected before and after the flight. The ambient light and sun irradiance data recorded by the DLS were utilized in the Pix4D calibration process. As suggested in the MicaSense Knowledge base, no additional

calibration of the thermal images was conducted in Pix4Dmapper, since the thermal camera is already radiometrically calibrated (*MicaSense Knowledge Base*, 2021).

Images were stitched together by Pix4Dmapper into orthomosaics using image keypoints. Keypoints are defining characteristics present in each photo. Once the orthomosaics were completed, the resulting maps were uploaded to QGIS for further analysis.

In QGIS, an orthomosaic map was uploaded for each band, resulting in six raster layers, Blue, Green, Red, NIR, Red edge, and LWIR. The Hydrolab sample locations were determined by uploading the KML file created by the GPS. The sample locations along the canoe path were determined by matching the times recorded by the GPS and the Hydrolab. Circular buffer points were created in QGIS at the determined sample locations, each with a 5-meter radius. The mean pixel value of each buffer point was collected using the QGIS zonal statistics feature. Since the images for the first five bands were monochromatic and normalized, the mean pixel values ranged between 0.00 and 1.00, with 0.00 indicating no reflectance and 1.00 total reflectance at the given wavelength. The thermal band, LWIR, mean values could be compared directly to the measured temperatures since the LWIR sensor pixel value outputs were in Centikelvin. The Centikelvin metadata was converted to Celsius using the provided equation given on the MicaSense Knowledge Base (*MicaSense Knowledge Base*, 2021).

$$T(℃) = 0.01(PV) - 273.15$$

Where T is temperature and PV is the pixel value in Centikelvin given by the camera (Simpson et al., 2021).

Using the mean pixel values from QGIS, different spectral indexes were created in a spreadsheet using the band calculations found in TABLE 2. The indexes analyzed were the Normalized Difference Vegetative Index (**NDVI**), Blue Normalized Difference Vegetative Index (**BNDVI**), Normalized Difference Red Edge Index (**NDRE**) (Kim et al., 2021), Normalized Difference Chlorophyll Index (**NDCI**) (Mishra & Mishra, 2012), an algorithm predicted by Landsat 7 data (**KAB_1A**) (Kabbara et al., 2008), Surface Algal Bloom Index (**SABI**) (Cillero Castro et al., 2020), a Two-Band Algorithm (**2BDA_1**) (Gitelson et al., 2008), a Three Band Algorithm (**3BDA**), and a Modified Three Band Algorithm (**3BDA_MOD**) (Dall'Olmo et al., 2003). Linear regression was performed on each of these indexes with the converted chlorophyll-a data in order to determine which index best fit the data. All points with the same phycocyanin reading from the Hydrolab were averaged before plotting to obtain a smoother trend. Outliers in the regression were determined and removed using a Thompson Tau test. The test led to 1-4 of 38 data points being outliers, depending on the index. The band arithmetic for each index can be seen in Table 2.

Index	Band Arithmetic	Bibliography Reference Number
NDVI	$\frac{(NIR - RED)}{(NIR + RED)}$	[3,4,7,9,10,15,19,33]
BNDVI	$\frac{(NIR - BLUE)}{(NIR + BLUE)}$	[7,10,19]
NDRE	$\frac{(NIR - REDEDGE)}{(NIR + REDEDGE)}$	[26,33]
NDCI	$\frac{(REDEDGE - RED)}{(REDEDGE + RED)}$	[4,36]
KAB_1a	$1.67 - 3.94\ln(BLUE) + 3.78\ln(\text{GREEN})$	[4,32]
SABI	$\frac{(NIR - RED)}{(BLUE + GREEN)}$	[4]
2BDA_1	$NIR\ /\ RED$	[4,34]
3BDA_1	$\left(\frac{1}{RED} - \frac{1}{REDEDGE}\right) * NIR$	[4,35]
3BDA_MOD	$\left(\frac{1}{RED} - \frac{1}{REDEDGE}\right)$	[4,35]

TABLE 2: Multispectral indexes used in chlorophyll-a analysis and reference to index literature.

3. Results

3.1 In-situ Measurements

The water quality data collected by the OTT Hydrolab were as expected for a freshwater lake in Minnesota. The 38 samples were collected by the Hydrolab with GPS location. For 34 of the 38 samples, buffer zones with 5m radiuses were created in QGIS. The other four samples were either measured by the probe outside the lake or too close to shore where a 5m zone could not be created.

	Temp [°C]	pH [Units]	LDO [mg/l]	PCYV [Volts]	Samples
Mean	21.5276	7.8750	9.7124	0.0111	34
Median	21.4100	7.8700	9.7000	0.0111	34
Range	0.9200	0.0500	0.2100	0.0018	34
St Dev	0.2704	0.0121	0.0472	0.0003	34

TABLE 3: Statistics of water quality data collected by the Hydrolab.

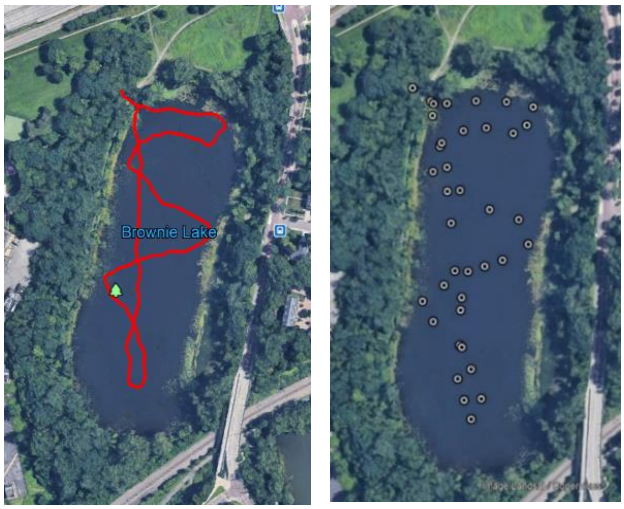

FIGURES 7 and 8: Canoe path taken on Brownie Lake (left) and Hydrolab sample locations (right). Path and Hydrolab sample locations were visualized using Google Earth

3.2 Chlorophyll-a Measurements

The results of the Standard method's chlorophyll-a extraction ranged between 0.67-8.72 $mg/m^3$of lake water. This data was consistent with publicly recorded chlorophyll-a concentrations for May in Brownie Lake (University of Minnesota, *Minnesota LakeBrowser*, 2021). The data resembled the years in which there was no recorded HAB on the surrounding lakes.

The chlorophyll-a data was then correlated to the phycocyanin levels recorded by the Hydrolab. The correlation was derived by recording the time of sample collection, then using the GPS data and averaging the phycocyanin measured volts before and after the sample collection. The resulting correlation was derived, with an R^2 value of 0.47.

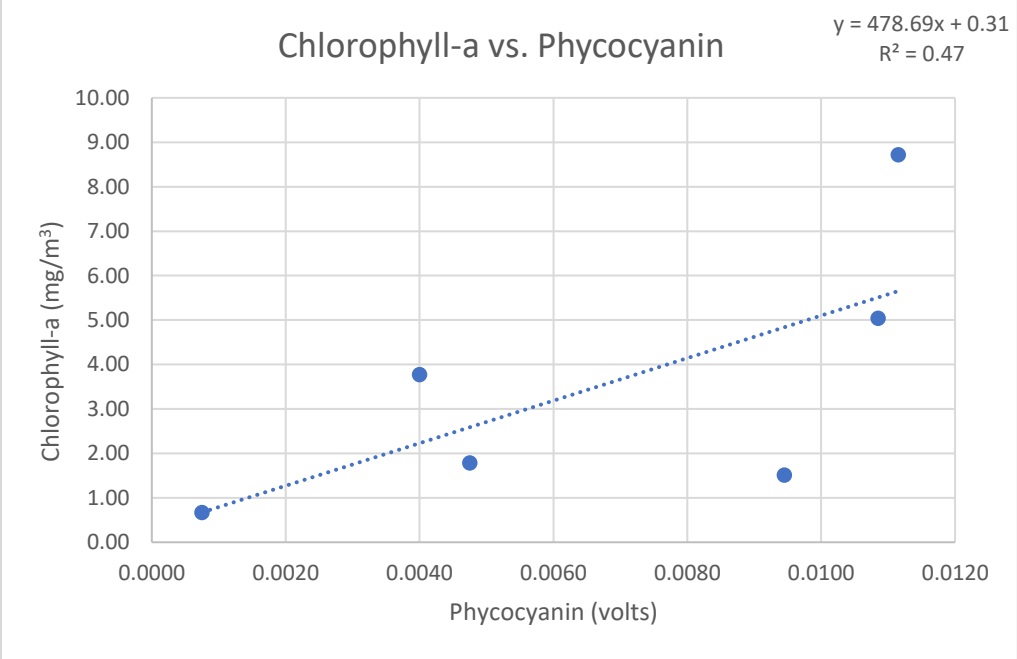

GRAPH 1: Linear relationship between chlorophyll extraction and phycocyanin concentration measured by the Hydrolab.

3.3 UAS Flight and Data

Weather conditions during UAS data collection included moderate cloud cover, gusts of wind with no precipitation. The flight was conducted between 3:00 and 4:00 pm CST. Drone data collection duration was 9 minutes and 22 seconds. The flight was 2,404 meters in length and covered an area of 0.111 km^2. During the flight, 164 images were captured for every sensor, resulting in a total of 984 images.

All images of Brownie Lake were properly stitched by the Pix4Dmapper software. The average number of key points per image was low at 7588 key points per image but were enough to stitch the photos together properly. Pix4D recommended an average of 10,000 key points per image; however, our result is sufficient for surveying a flat homogenous surface like a lake. The orthomosaics had high overlap and were adequate for creating indexes for analysis. The experimental average ground sample distance was 4.57 cm for the multispectral sensors. With a GSD of 4.57 cm, each pixel covered an area of 20.9 cm^2. Due to the much lower resolution, the thermal sensor had a recorded GSD of 71 cm. Pix4Dmapper uses the highest resolution available data when creating the orthomosaics. Therefore, the lower resolution of the thermal sensor did not negatively impact the thermal orthomosaic since it was stitched using the higher resolution multispectral images as references.

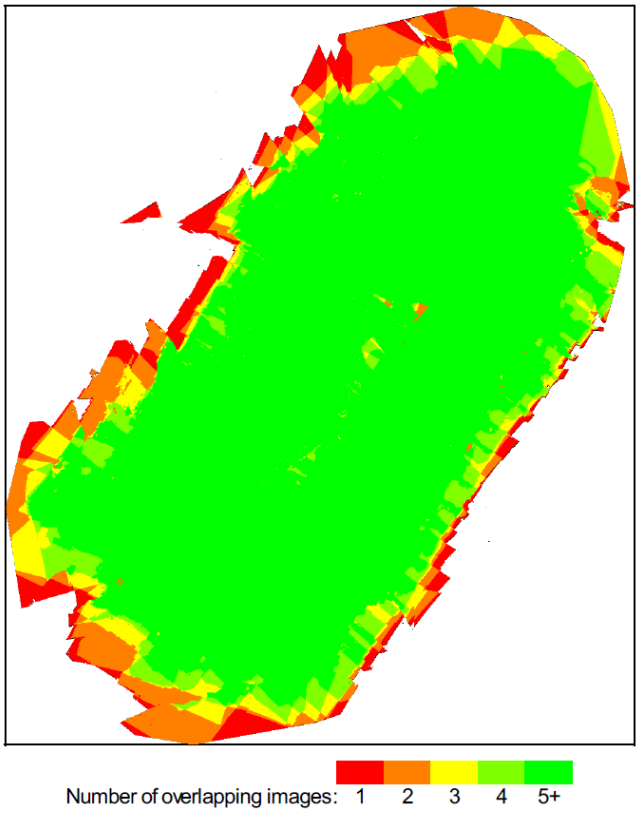

FIGURE 9: Image overlap of the orthomosaic of Brownie Lake. Image generated by Pix4D Quality Report.

3.4 Spectral Indexes and Chlorophyll-a

The index with the strongest correlation to chlorophyll concentration was NDVI with an $R^2 = 0.80$ **(Table 4)**. Many of the other indexes also showed a strong correlation with the determined chlorophyll-a concentration. The four indexes with the highest R^2 were NDVI, BNDVI, 2BDA_1, and SABI, which all contained the NIR band. This suggests that the NIR is the most correlated with water chlorophyll-a concentration. NDVI, 2BDA_1, and SABI were combinations of only the NIR and red bands. Therefore, three out of the four indexes with the most significant correlation were NIR and red bands combinations. This would agree with other previous studies that have also shown a

strong correlation of chlorophyll-a concentration and combinations of NIR and red bands (Cillero Castro et al., 2020). Indexes that contained the combination of the red-edge and red bands also showed a good correlation, but not as much as those containing the NIR and red bands.

Outliers in the regression were determined and removed using a Thompson Tau test. This resulted in 2-3 outliers, depending on the index, out of the 34 buffer points. Due to the large amounts of samples with the same phycocyanin reading, the mean pixel values were averaged for all samples that produced the same phycocyanin reading from the Hydrolab. The remaining values were plotted against the data from the Hydrolab, which resulted in the correlations seen in Table 4. After averaging all points with the same phycocyanin reading from the Hydrolab and removing outliers, there were 10-11 data points left depending on the index. The resulting NDVI correlation was then entered into QGIS, creating a new orthomosaic of chlorophyll-a concentration.

$$Chlorophyll - a\ (mg/m^3) = 10.90(NDVI) + 8.92$$

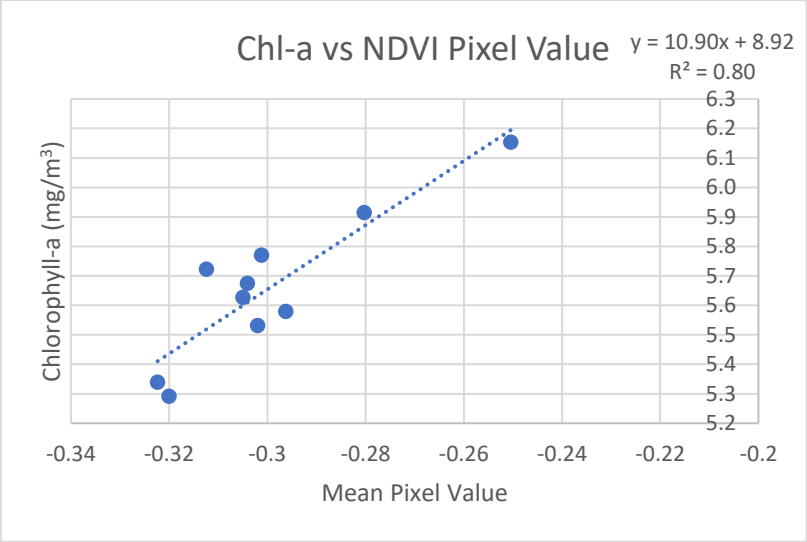

GRAPH 2: Correlation between chlorophyll-a concentration and mean NDVI pixel value.

Index	Band Arithmetic	Number of Outliers	Number of Data Points	R^2 Value
NDVI	$\frac{(NIR - RED)}{(NIR + RED)}$	2	10	$R^2 = 0.80$
BNDVI	$\frac{(NIR - BLUE)}{(NIR + BLUE)}$	2	10	$R^2 = 0.74$
NDRE	$\frac{(NIR - REDEDGE)}{(NIR + REDEDGE)}$	2	10	$R^2 = 0.57$
NDCI	$\frac{(REDEDGE - RED)}{(REDEDGE + RED)}$	3	10	$R^2 = 0.55$
KAB	$1.67 - 3.94\ln(BLUE) + 3.78\ln(\mathrm{GREEN})$	3	11	$R^2 = 0.47$
SABI	$\frac{(NIR - RED)}{(BLUE + GREEN)}$	2	10	$R^2 = 0.68$
2BDA_1	NIR/RED	2	10	$R^2 = 0.71$
3BDA_1	$\left(\frac{1}{RED} - \frac{1}{REDEDGE}\right) * NIR$	3	10	$R^2 = 0.46$
3BDA_ MOD	$\left(\frac{1}{RED} - \frac{1}{REDEDGE}\right)$	3	10	$R^2 = 0.60$

TABLE 4: R^2 values for linear regression of each band index listed.

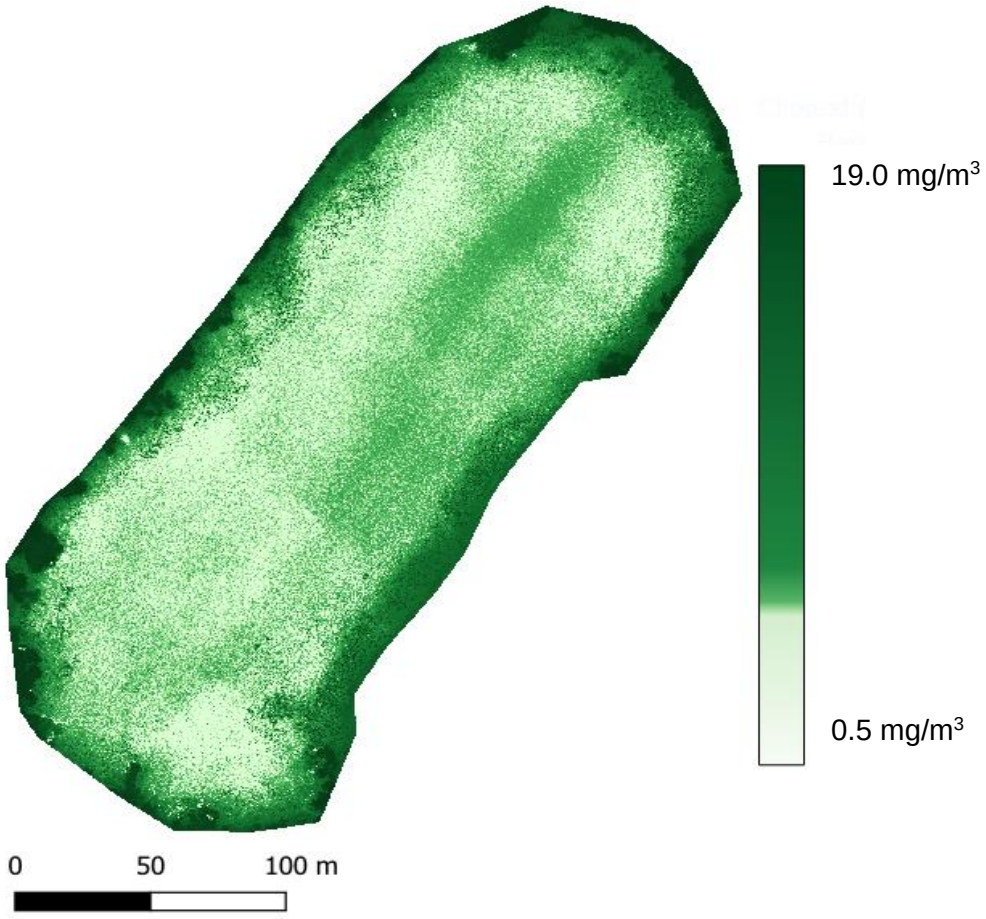

FIGURE 11: Contour map of chlorophyll concentration in Brownie Lake.

Using the NDVI, the UAS calculated average chlorophyll-a value was 6.96 mg/m^3, with a median of 5.77 mg/m^3, RMSE of 3.07 mg/m^3, and a range of 18.22 mg/m^3. Using a Z value of 1.96, the 95% confidence intervals for this model were 0.94 mg/m^3 and 12.98 mg/m^3. The distribution of chlorophyll tapered off slowly. The discrepancy between the mean and median chlorophyll-a concentrations can be seen in the fat-tail of the distribution. The observed chlorophyll-a concentration is most concentrated along the shore of the lake.

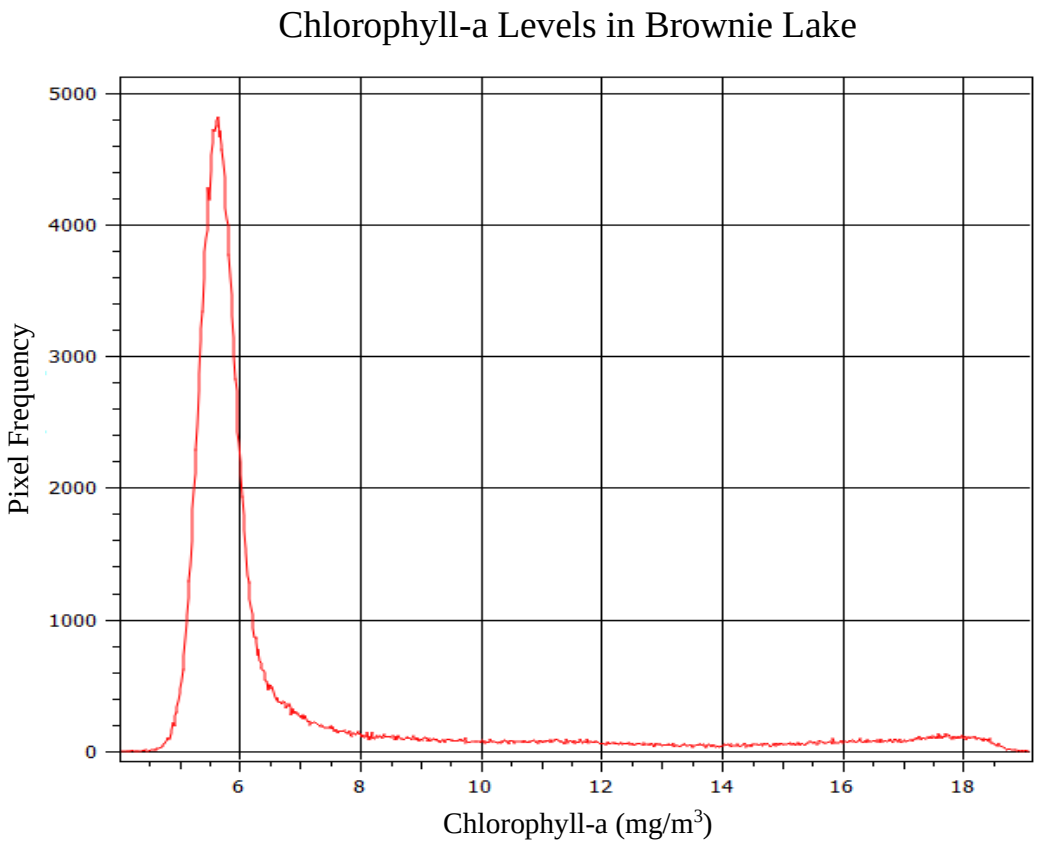

GRAPH 3: Histogram showing the range of chlorophyll-a concentrations in Brownie Lake per pixel (20.9 cm^2). Pixel frequency is the number of pixels with the corresponding chlorophyll-a value.

The areas with the most concentrated chlorophyll-a readings on the map were tree branches hanging over the lake and were still present after cropping the image. The trees are observed as dark green figures in the contour map along the shoreline. Leaves have very large NDVI values because leaves are full of chlorophyll, meaning they reflect NIR light and absorb red light. Another problem was the leaves that fell from the trees onto the lake surface. While conducting the survey, many leaves were observed on the lake surface, and leaves are also observed on the lake surface in the NDVI orthomosaic. The

branches and leaves are the most likely cause for the extensive range of values observed. The two outliers omitted from the linear regression analysis were two buffer zones close to the shoreline where the water surface was covered with leaves. Due to the trees and the leaves on the lake surface, there are many pixels with high chlorophyll-a values causing the histogram to resemble a fat tail distribution.

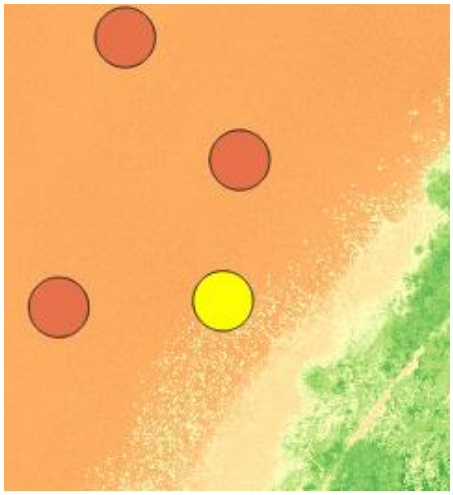

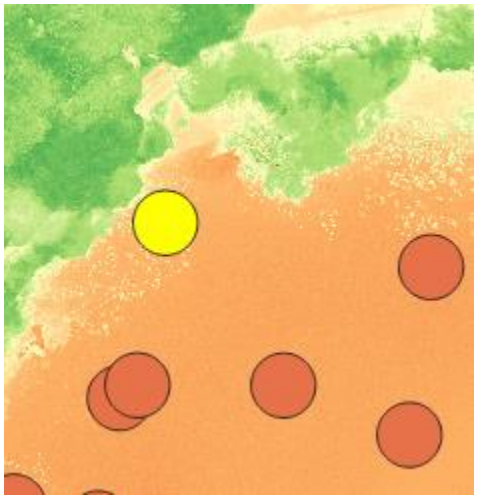

FIGURES 11 and 12: NDVI with buffer zone 20 (left) and 34 (right). Zone 20 and 34 were marked as outliers by the Thompson Tau test. Leaves can be seen as yellow pixels near the zones and along the shoreline.

3.5 UAS Thermal Temperatures

UAS recorded temperature by the LWIR thermal camera measured a mean temperature of 18.68 °C with an RMSE of 1.82 °C. The temperature map of the lake created by the thermal camera was uniform. However, the range calculated directly from the camera was 33.50 °C. The calculated range was so large due to the maximum

recorded value, 48.77 °C. The large range did not agree with the observed Hydrolab measured temperatures, which reported consistently higher temperatures.

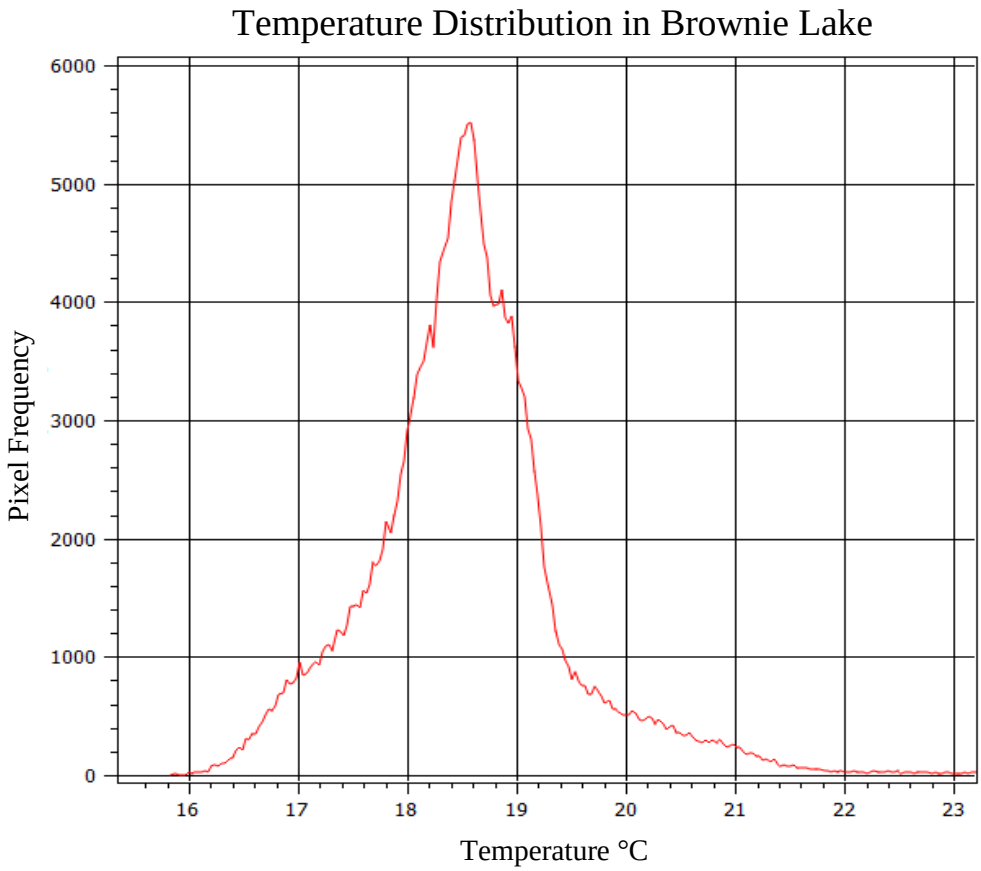

GRAPH 4: Raw LWIR pixel data converted to °C from Centikelvin.

The phenomenon of thermal sensors reporting lower temperature values has been observed by other academics who have attempted to measure water surface temperatures by UASs. The lower temperatures are attributed to different environmental stressors, including wind speed, which can cool the camera lens, and high humidity absorbing the LWIR bands (Jensen et al., 2012). While this data may be suitable for some uses, the accuracy was improved by matching the values to the probe measured temperatures from

the Hydrolab. Another linear regression was performed between the UAS measured temperatures and the Hydrolab probe measured temperatures. The correlation is shown in GRAPH 5.

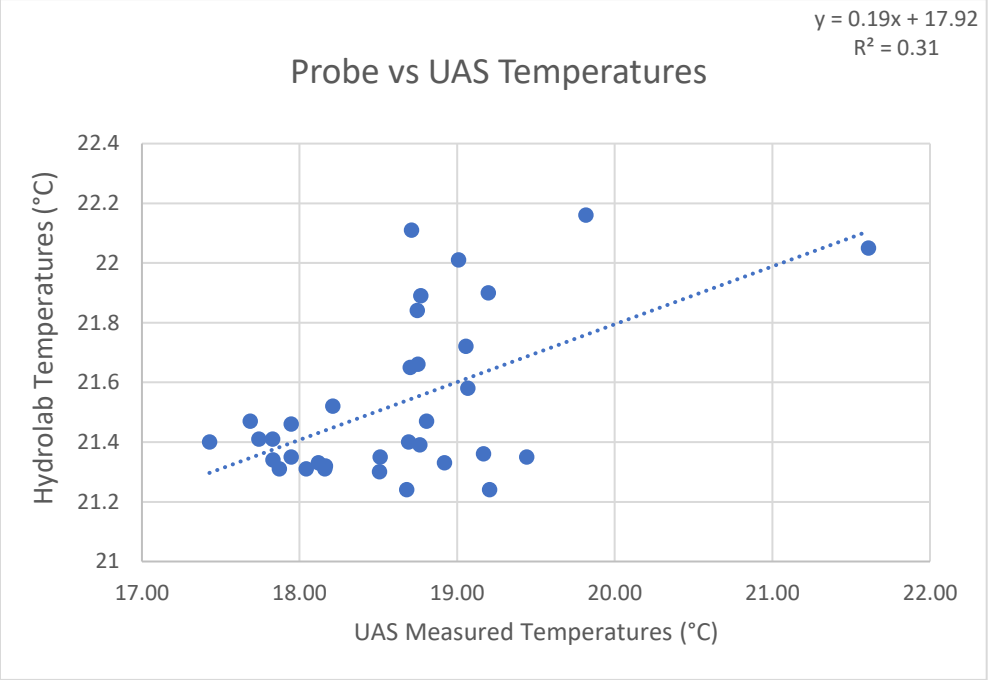

GRAPH 5: UAS collected temperatures versus Hydrolab probe measured temperatures.

Another thermal map was created in QGIS using the correlation in GRAPH 5. Due to the much lower resolution of the LWIR thermal sensor, a less detailed map was produced when compared to the multispectral indexes. The resulting histogram not only matched the Hydrolab data but had a much smaller range of 6.49 °C, despite the low R^2 value. The max pixel value after the regression was 27.37 °C. When compared to the probe measured temperatures, the initial data was within the manufacturer's specifications found in the MicaSense Altum Integration guide, +/- 5K (MicaSense, 2020).

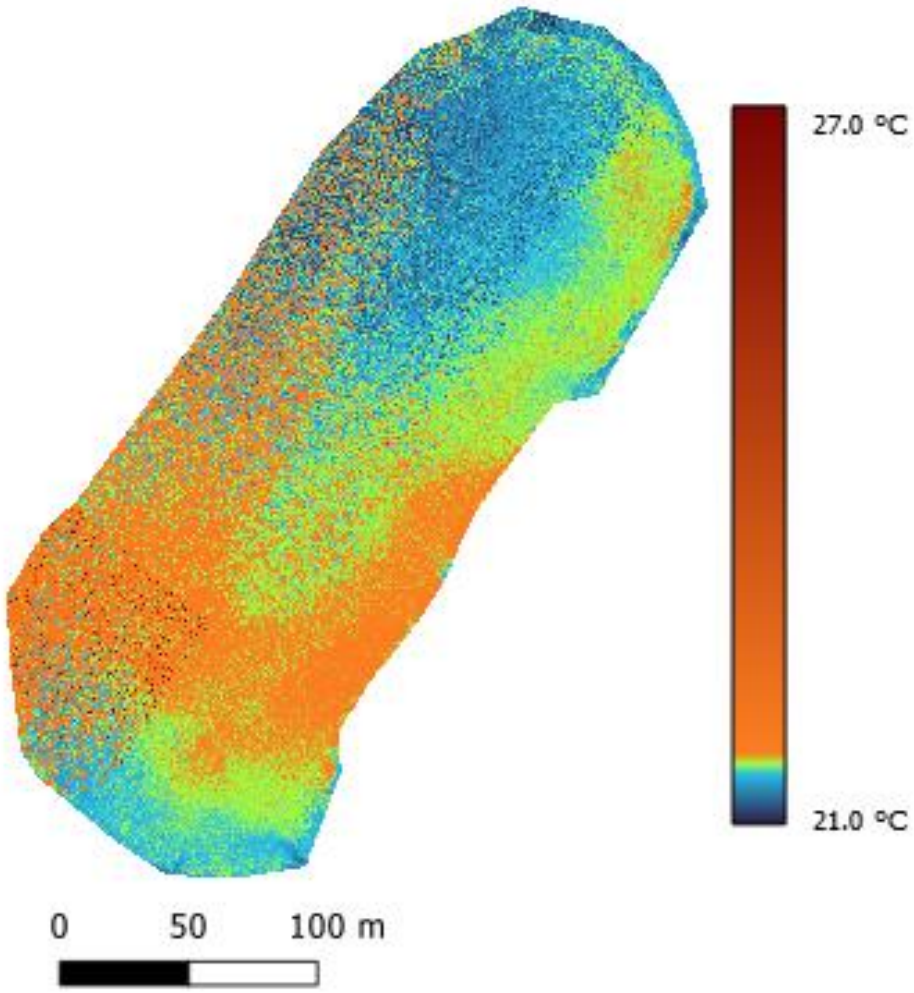

FIGURE 13: Thermal temperature map of Brownie Lake post regression analysis**.**

The thermal map shows the warmest temperatures, on average, are closer to the shoreline. The exceptions to this rule are the north and south shores, both of which are shaded with trees. The regression analysis brought the range of temperatures down to an acceptable and expectable range. While the thermal camera collected lots of data rapidly, the raw data collected by the LWIR sensor is not accurate enough on its own to be acceptable for all uses.

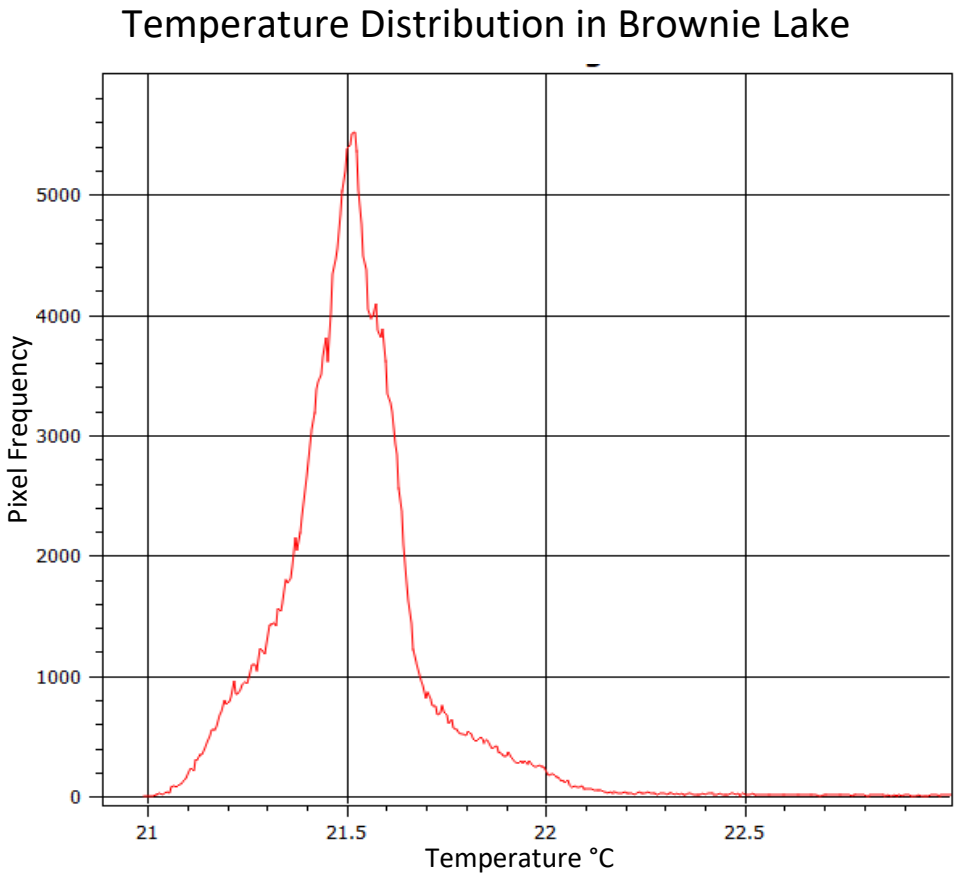

GRAPH 6: Histogram of water temperatures in Brownie Lake, post regression analysis. Pixel frequency is the number of pixels with the corresponding temperature value.

4. Discussion

4.1 UAS Determination of Algae Concentration

Measuring chlorophyll-a and phycocyanin concentration by multispectral UAS imagery were shown to be effective methods for measuring the distribution of phytoplankton in freshwater lakes. Multiple spectral indexes were shown to be correlated with the in-situ measured phycocyanin levels and lab-determined chlorophyll-a concentrations. The NIR band showed the highest correlation with in-situ measurements. Other studies discovered a similar result, with the red and NIR bands being highly correlated for low chlorophyll-a concentrations (0-10 mg/m^3) (Cillero Castro et al., 2020). This concept is supported by many decades of research into remote sensing chlorophyll by satellites. This confirms the findings of other studies using UAS multispectral indexes to monitor algae populations (Wu et al., 2019).

UAS imagery proved to offer on-demand data at a higher resolution than other remote sensing methods. UAS imagery also benefits from being less time, position, and weather dependent than traditional remote sensing methods. In this research, accurate indexes were obtained regardless of cloud cover. Since a UAS is much closer to the field of interest than a satellite, the effects of atmospheric interference are minimal compared to a satellite (Tmušić et al., 2020).

This research opens up the possibility for real-time water quality monitoring and allows for the measurement of chlorophyll flux throughout surface waters. This technology could allow for the tracking of HABs in small bodies of water as they develop. Higher image resolution naturally provided more detail of the water, which

allowed for a potential source for statistical outliers, the leaves on the water surface, to be identified and accounted for in the analysis. The high resolution also provides the opportunity to measure water bodies that are too small to observe with satellites, such as streams or rivers (Choo et al., 2018).

However, the added benefits from UAS imagery come at a tradeoff. Brownie Lake worked for this survey because it was long, narrow, and calm. The calm water played a role in keeping the flux of phytoplankton low throughout the analysis. If data collection time was longer or if the water is moving faster, the flux of plankton may affect the result of the data.

Many algae species that cause HABs can lie below the surface (Kwon et al., 2019). Given that algae can migrate vertically, the data received by the UAS sensor is highly dependent on the surface level algae concentration (Kislik et al., 2018). However, this particular issue is not specific to UAS remote sensing.

The MicaSense Altum was designed to collect agriculture data, and that is where it excels. After applying this technology to water quality, it is clear it has limitations in its current capacity. The most significant problem encountered in this research was the lack of defining features in the images collected by the camera. The images need these defining features if the images are to be stitched together correctly. Uniformity is inherent to calm water surfaces, so some of the collected images naturally lacked defining features.

Certain water bodies with high levels of roughness also encounter the problem of waves changing the water surface between photo intervals (Gitelson et al., 2008). This problem is commonly observed when taking a digital panoramic photo of any moving

water. Most of the images collected from the survey had enough defining features from the shoreline present in the images to be stitched correctly. The stitching process introduced uncertainties that would not be present in a singular photo collected by satellite. This method would be most effectively utilized in waters with defining features such as wetlands, shorelines, or small rivers. Increasing the flight height of the drone would lower the resolution but would help to capture more defining features in each photo. Future research needs to be conducted on different photo stitching methods, such as hyper-precise geotagging, that do not need to rely on defining features of images.

This study could have benefited from more in-situ chlorophyll-a measurements. While the correlation between phycocyanin and chlorophyll-a was significant in this study, this will not always be the case with other water bodies that contain high levels of non-cyanobacteria phytoplankton because phycocyanin is specific to cyanobacteria. OTT Hydromet does recommend using the phycocyanin sensor for freshwater with large populations of cyanobacteria or when cyanobacteria are of particular interest (Sanders et al., 2000). Due to the 2020 cyanobacteria bloom on the neighboring lake, cyanobacteria were of specific interest; therefore, the use phycocyanin sensor was appropriate for this study. However, an additional chlorophyll-a probe would give this study more insight into the relationship between phycocyanin and chlorophyll-a in Brownie Lake.

4.2 UAS Determination of Surface Water Temperature

UAS LWIR thermal technology was shown to be a method one could employ to acquire thermal maps of small bodies of water. The technology is promising but had significant enough errors, in our study, that the pixel values had to be matched with in-

situ measured temperatures. Further research needs to be conducted on the environmental stressors that lead to the lower readings observed by the thermal camera versus data collected on the ground. These lower UAS determined temperatures are observed in other studies of water surface temperature (Jensen et al., 2012) but not observed when surveying land (Simpson et al., 2021). This indicates the need for further development of an algorithm or new thermal camera specifically catered to the needs of remote sensing water surface temperature with LWIR technology. The problem appears to be specific to water surfaces, so additional atmospheric interferences should be investigated. This interference may be the result of the air-water interface or vapor pressure above the water surface.

Using a thermal camera in this study allowed a thermal map to be created quickly, something difficult to accomplish with manually measured temperatures. The thermal map allowed for creating a histogram with a massive number of temperature samples (22,154,32 pixels), a number not easily achieved by other methods. The thermal sensor was within the manufacturer specification of +/- 5K (MicaSense, 2020) for all mean pixel values of buffer points when compared to the Hydrolab measured temperatures. The LWIR sensor had the benefit of being attached to higher resolution multispectral sensors. The higher resolution of the multispectral sensors allowed for the generation of a more accurate thermal orthomosaic than would be possible with the thermal sensor alone. This is one of the advantages observed in using a thermal-multispectral combination camera, like the MicaSense Altum.

While this discrepancy may be tolerable for specific applications, the results were drastically improved after regression analysis. Despite the lower accuracy, this research

does show proof of concept for measuring water surface temperatures with LWIR thermal sensors. Additional research is needed to increase the accuracy of these measurements. This technology could benefit from the development of thermal cameras that are specifically designed for monitoring surface water temperatures by UASs.

4.3 Conclusions

This study shows the potential use case for UAS monitoring of water quality in small inland lakes. Chlorophyll-a concentrations in water were shown to be correlated with many spectral indexes, including commonly used indexes such as NDVI. Due to chlorophyll's strong absorption of red light and reflectance of NIR light, NDVI has been used for many years to estimate vegetation vigor. Our analysis shows that this index is also correlated with chlorophyll-a concentration in surface waters. Through analysis of the indexes, the NIR band (842 nm) was shown to have the most significant correlation with measured phytoplankton biomass. These results support other studies of UAS multispectral water quality analysis.

There is a major use case in using UAS technology to monitor eutrophic HABs. While the correlation is strong, the technology still heavily depends on in-situ data to produce accurate results. Further study is needed on index correlation over a more extensive range of chlorophyll-a measurements. The scope of this project focused on low chlorophyll-a concentrations and did not measure any eutrophic waters. Therefore, providing a correlation over large chlorophyll-a concentrations would be immensely useful. The water in Brownie Lake was not highly turbid either. Additional research into how turbidity affects multispectral and thermal measurements captured by UASs sensors

is needed to understand their viability for lakes with differing trophic states (Gitelson et al., 2008).

The MicaSense Altum also showed future potential for remote sensing water surface temperature by LWIR sensors. This technology could see actual use in monitoring surface water temperatures of lakes and rivers. UAS thermal imagery could help show temperature fluxes through small water bodies, something satellite spatial resolution cannot observe. Observing the temperatures of lakes and rivers is crucial to environmental monitoring since temperature dictates the rate of chemical and biological processes in natural waters. If water temperatures are shown to be higher than usual, a HAB could occur. UAS thermal sensors are much more efficient at collecting temperature data on a mass scale. This technology also could be useful in monitoring thermal water pollution near dams or powerplants, where temperatures may differ over short areas. Research with UAS thermal cameras has already shown the effects of dams on temperature distribution in rivers (Jensen et al., 2012).

UAS technology proves to be another valuable tool for the environmental monitoring of surface waters. Due to the higher resolution of imagery produced, this new technology has a lot of potential for observing bodies of water that are too small for traditional methods of remote sensing. Additional research needs to be conducted to determine if UAS multispectral imagery can play an important role in monitoring or predicting HABs. In-situ data should be collected and incorporated into the analysis to collect the most accurate data from a UAS multispectral or thermal sensor. More research development needs to be conducted so that future UAS sensors do not need to rely so heavily on ground collected data.

UAS imagery can provide real-time data, which can help environmental issues be addressed quickly. There would be much potential for monitoring surface waters by UASs, especially if a UAS sensor were specifically designed for monitoring water quality. Using UAS technology provides flexible, affordable, rapid mass data collection that can prove incredibly useful when protecting the water resources in our environment.

Bibliography

1. Wynne, T., A. Meredith, T. Briggs, W. Litaker, and R. Stumpf 2018. *Harmful Algal Bloom Forecasting Branch Ocean Color Satellite Imagery Processing Guidelines*. NOAA Technical Memorandum NOS NCCOS 252. Silver Spring, MD. 48 pp. doi:10.25923/twc0-f025

2. Arango, J. G., & Nairn, R. W. (2019). *Prediction of Optical and Non-OpticalWater Quality Parameters in Oligotrophic and Eutrophic Aquatic Systems Using a Small Unmanned Aerial System*. Drones, 4.

3. Choo, Y., Kang, G., Kim, D., & Lee, S. (2018). *A study on the evaluation of water-bloom using image processing*. Environmental Science and Pollution Research, 25, 36775–36780.

4. Cillero Castro, C., Domínguez Gómez, J. A., Delgado Martín, J., Hinojo Sánchez, B. A., Cereijo Arango, J. L., Cheda Tuya, F. A., & Díaz-Varela, R. (2020). *An UAV and Satellite Multispectral Data Approach to Monitor Water Quality in Small Reservoirs. Remote Sensing*, 12.

5. Crabb, R. C. (2020). *2020 Spring Algae Bloom Event Report*. 2.

6. Fricke, K., Baschek, B., Jenal, A., Kneer, C., Weber, I., Bongartz, J., Wyrwa, J., & Schöl, A. (2021). *Observing Water Surface Temperature from Two Different Airborne Platforms over Temporarily Flooded Wadden Areas at the Elbe Estuary—Methods for Corrections and Analysis*. Remote Sensing, 13.

7. Guimarães, T., Veronez, M., Koste, E., Gonzaga, L., Bordin, F., Inocencio, L., Larocca, A., de Oliveira, M., Vitti, D., & Mauad, F. (2017*). An Alternative Method of Spatial Autocorrelation for Chlorophyll Detection in Water Bodies Using Remote Sensing*. Sustainability, 9.

8. Jensen, A. M., Neilson, B. T., McKee, M., & Chen, Y. (2012). *Thermal remote sensing with an autonomous unmanned aerial remote sensing platform for surface stream temperatures*. 5049–5052.

9. Kim, W., Jung, S., Moon, Y., & Mangum, S. C. (2020). *Morphological Band Registration of Multispectral Cameras for Water Quality Analysis with Unmanned Aerial Vehicle*. Remote Sensing, 12.

10. Kislik, C., Dronova, I., & Kelly, M. (2018). *UAVs in Support of Algal Bloom Research: A Review of Current Applications and Future Opportunities*. Drones, 2.

11. Kwon, Y. S., Pyo, J., Kwon, Y.-H., Duan, H., Cho, K. H., & Park, Y. (2019). *Drone-Based Hyperspectral Remote Sensing of Cyanobacteria Using Vertical Cumulative Pigment Concentration in a Deep Reservoir*. Remote Sensing of Environment.

12. Obenour, D., Gronewold, D., Stow, C., & Scavia, D. (2014). *2014 Lake Erie Harmful Algal Bloom (HAB)* Experimental Forecast: This product represents the first year of an experimental forecast relating bloom size to total phosphorus load. 2.

13. Price, J. C. (1983). *Estimating Surface Temperatures from Satellite Thermal Infrared Data—A Simple Formulation for the Atmospheric Effect*. Remote Sensing of Environment, 13, 353–361.

14. Simpson, J. E., Holman, F., Nieto, H., Voelksch, I., Mauder, M., Klatt, J., Fiener, P., & Kaplan, J. O. (2021). *High Spatial and Temporal Resolution Energy Flux Mapping of Different Land Covers Using an Off-the-Shelf Unmanned Aerial System*. Remote Sensing, 13.

15. Taddia, Y., Russo, P., Lovo, S., & Pellegrinelli, A. (2020). *Multispectral UAV monitoring of submerged seaweed in shallow water*. Applied Geomatics, 12, 19–34.

16. Tmušić, G., Manfreda, S., Aasen, H., James, M. R., Gonçalves, G., Ben-Dor, E., Brook, A., Polinova, M., Arranz, J. J., Mészáros, J., Zhuang, R., Johansen, K., Malbeteau, Y., de Lima, I. P., Davids, C., Herban, S., & McCabe, M. F. (2020). *Current Practices in UAS-based Environmental Monitoring*. Remote Sensing, 12.

17. *What is a harmful algal bloom?* | National Oceanic and Atmospheric Administration. (2016). Retrieved from https://www.noaa.gov/what-is-harmful-algal-bloom

18. Woźniak, M., Bradtke, K., Darecki, M., & Krężel, A. (2016*). Empirical Model for Phycocyanin Concentration Estimation as an Indicator of Cyanobacterial Bloom in the Optically Complex Coastal Waters of the Baltic Sea*. Remote Sensing, 8.

19. Wu, D., Li, R., Zhang, F., & Liu, J. (2019). *A Review on Drone-Based Harmful Algae Blooms Monitoring*. Environmental Monitoring and Assessment, 191, 211.

20. Day, R. A. (1988). *How to Write and Publish a Scientific Paper* (3rd ed.). Oryx Press.

21. MicaSense. (2020). *MicaSense Altum and DLS 2 Integration Guide*. 10.

22. MicaSense. (2021). *User Guide for MicaSense Sensors*. 9.

23. Sanders, P., & Hydromet, H. (2000). *An Introduction to Algae Measurements Using In Vivo Fluorescence*. OTT Hydrolab.

24. *Standard Methods for the Examination of Water and Wastewater* (19th ed.). (1995).

25. Cardwell, J. (2020, May 15). *The Algae Bloom On Minneapolis' Cedar Lake Is Likely Harmful*. https://minnesota.cbslocal.com/2020/05/15/the-algae-bloom-on-minneapolis-cedar-lake-is-likely-harmful/

26. *MicaSense Knowledge Base*. (2021). Retrieved from https://support.micasense.com/hc/en-us

27. *Minnesota LakeBrowser*. (2021). https://lakes.rs.umn.edu/#27003800. University of Minnesota Remote Sensing of Water Resources.

28. *Satellites See Red, Blue and Green: Monitoring Harmful Algal Blooms from Space | NOAA National Environmental Satellite, Data, and Information Service (NESDIS)*. (2015). Retrieved from https://www.nesdis.noaa.gov/content/satellites-see-red-blue-and-green-monitoring-harmful-algal-blooms-space

29. Kislik, C., Dronova, I., & Kelly, M. (2018). *UAVs in Support of Algal Bloom Research: A Review of Current Applications and Future Opportunities*. Drones, 2.

30. Wu, D., Li, R., Zhang, F., & Liu, J. (2019). *A review on drone-based harmful algae blooms monitoring. Environmental Monitoring and Assessment*, 191, 211.

31. Kwon, Y. S., Pyo, J., Kwon, Y.-H., Duan, H., Cho, K. H., & Park, Y. (2019). *Drone-based hyperspectral remote sensing of cyanobacteria using vertical cumulative pigment concentration in a deep reservoir*. Remote Sensing of Environment.

32. Nijad Kabbara, Jean Benkhelil, Mohamed Awad, Vittorio Barale, (2008). *Monitoring water quality in the coastal area of Tripoli (Lebanon) using high-resolution satellite data. ISPRS Journal of Photogrammetry and Remote Sensing*. Volume 63, Issue 5, Pages 488-495, ISSN 0924-2716.

33. Kim, E.-J., Nam, S.-H., Koo, J.-W., & Hwang, T.-M. (2021). *Hybrid Approach of Unmanned Aerial Vehicle and Unmanned Surface Vehicle for Assessment of Chlorophyll-a Imagery Using Spectral Indices in Stream, South Korea*. Water, 13(14), 1930.

34. Gitelson, A. A., Dall'Olmo, G., Moses, W., Rundquist, D. C., Barrow, T., Fisher, T. R., Gurlin, D., & Holz, J. (2008). *A simple semi-analytical model for remote estimation of chlorophyll-a in turbid waters: Validation*. Remote Sensing of Environment, 112(9), 3582–3593.

35. Dall'Olmo, G., Gitelson, A. A., & Rundquist, D. C. (2003). *Towards a unified approach for remote estimation of chlorophyll-a in both terrestrial vegetation and turbid productive waters: UNIFIED APPROACH FOR CHLOROPHYLL ESTIMATION*. Geophysical Research Letters, 30(18).

36. Mishra, S., & Mishra, D. R. (2012). *Normalized difference chlorophyll index: A novel model for remote estimation of chlorophyll-a concentration in turbid productive waters.* Remote Sensing of Environment, 117, 394–406.

37. FLIR. (2018). *Lepton with Radiometry Quickstart Guide*.

38. FLIR. (2018). FLIR Lepton 3 & 3.5.

39. Schmale, D. G., Ault, A. P., Saad, W., Scott, D. T., & Westrick, J. A. (2019). *Perspectives on Harmful Algal Blooms (HABs) and the Cyberbiosecurity of Freshwater Systems.* Frontiers in Bioengineering and Biotechnology, 7, 128.